RAA 2021 Vol. **21** No. **10**, 267(11pp) doi: 10.1088/1674-4527/21/10/267

http://www.raa-journal.org *http://iopscience.iop.org/raa*

Research in Astronomy and Astrophysics

Solar observation with the Fourier transform spectrometer I : Preliminary results of the visible and near-infrared solar spectrum

Xian-Yong Bai (白先勇)[1,2], Zhi-Yong Zhang (张志勇)[1,2], Zhi-Wei Feng (冯志伟)[1,2], Yuan-Yong Deng (邓元勇)[1,2], Xing-Ming Bao (包星明)[1], Xiao Yang (杨潇)[1], Yong-Liang Song (宋永亮)[1], Li-Yue Tong (佟丽越)[1,2] and Shuai Jing (荆帅)[1]

[1] Key Laboratory of Solar Activity, National Astronomical Observatories, Chinese Academy of Sciences,Beijing 100101, China; *xybai@bao.ac.cn*

[2] School of Astronomy and Space Science, University of Chinese Academy of Sciences, Beijing 101408, China

Received 2021 February 10; accepted 2021 July 11

Abstract The Fourier transform spectrometer (FTS) is a core instrument for solar observation with high spectral resolution, especially in the infrared. The Infrared System for the Accurate Measurement of Solar Magnetic Field (AIMS), working at 10–13 μm, will use an FTS to observe the solar spectrum. The Bruker IFS-125HR, which meets the spectral resolution requirement of AIMS but simply equips with a point source detector, is employed to carry out preliminary experiment for AIMS. A sun-light feeding experimental system is further developed. Several experiments are taken with them during 2018 and 2019 to observe the solar spectrum in the visible and near infrared wavelength, respectively. We also proposed an inversion method to retrieve the solar spectrum from the observed interferogram and compared it with the standard solar spectrum atlas. Although there is a wavelength limitation due to the present sun-light feeding system, the results in the wavelength band from 0.45–1.0 μm and 1.0–2.2 μm show a good consistency with the solar spectrum atlas, indicating the validity of our observing configuration, the data analysis method and the potential to work in longer wavelength. The work provided valuable experience for the AIMS not only for the operation of an FTS but also for the development of its scientific data processing software.

Key words: Sun: general — methods: observational — instruments: Fourier transform spectrometer

1 INTRODUCTION

Astronomical spectrum provides us a unique opportunity to quantitatively investigate the physical parameters of the observed objects, e.g., chemical composition, temperature, abundance, line-of-sight velocity, pressure and the magnetic field, and so on (Tennyson 2011). Up to now, most of the knowledge we learned about the Sun, our nearest star, comes from the spectral observations. With the solar spectropolarimetry data, we are able to derive up to tens of physical parameters and even their variation with optical depth with the help of powerful inversion techniques (del Toro Iniesta & Ruiz Cobo 2016; Ai 1993; Socas-Navarro et al. 2015). We can then reconstruct the dynamical three-dimensional solar atmosphere so as to better understand different kinds of quiet or active solar phenomena, such as sunspots, granulation as well as solar flares (Fang et al. 2010; Feng et al. 2020; Xu et al. 2005; Li et al. 2017).

Infrared solar spectrum contains lots of scientific advantages relative to the other wavelength. First, it is helpful for the accurate measurements of solar magnetic fields. The ability of a magnetic sensitive line is generally represented by Zeeman sensitivity, which is the ratio of the Zeeman splitting divided by the spectral line width and proportional to $g\lambda$ (Penn 2014). Here g is the Landé factor of the selected spectral line and λ is the wavelength. If the infrared lines with larger λ are used, we can get much higher Zeeman sensitivity (Bruls et al. 1995; Solanki et al. 2006). Secondly, many molecular rotation-vibrations lines exist in the infrared waveband and provide unique ways to probe the cool parts of the solar atmosphere, e.g., the well known CO lines near 4.6 microns (Ayres 2002; Solanki et al. 1994; Uitenbroek et al. 1994; Li et al. 2020). Lastly, we can also probe different heights of the solar atmosphere only using continuum radiation because the infrared wavelength covers a wide range from 0.7 to 1000 µm (Penn 2014). So most of the new constructed solar telescopes are equipped with the post-focus instrument working in the infrared wavelength, such as the cryogenic infrared spectrograph (CYRA) for the Goode Solar Telescope (GST) and the Cryogenic Near-Infrared Spectro-Polarimeter for the Daniel K. Inouye Solar Telescope (Cao et al. 2010; Rimmele et al. 2020). We will usher in a golden age for solar infrared observation in the coming decades.

To accurately measure solar magnetic fields, a new telescope named the Infrared System for the Accurate Measurement of Solar Magnetic Field (AIMS) is under construction in China. The Mg I 12.32 µm line is selected as the working line because it has the largest magnetic sensitivity among our known spectral lines so far. The required spectral resolution is 0.6 Å at 12.32 µm (Deng et al. 2016), with a resolution power of 205 333. AIMS employs the Fourier transform spectrometer (FTS) to realize the high resolution power. In the 1980s, McMath−Pierce Solar Facility at National Solar Observatory, USA, also used an FTS to discover the Mg I 12.32 µm line (Brault 1972, 1978; Chang & Noyes 1983). In addition, the FTS is employed by many solar spaceborne missions to obtain the middle and far infrared solar spectrum, e.g., the ATMOS (Atmospheric Trace Molecule Spectroscopy) experiment on Spacelab 3, and the ACE-FTS (Atmospheric Chemistry Experiment) onboard the Canadian SCISAT-1 satellite (Hase et al. 2010; Farmer & Norton 1989; Farmer 1994).

Unfortunately, the FTS has never been used by any solar telescopes in China in the past. Hence one of the main problems encountered by AIMS is how to obtain solar spectrum with an FTS. In the paper, we carried out an experiment aiming to observe the solar spectrum with our newly installed FTS at Huairou Solar Observing Station (HSOS), National Astronomical Observatories, Chinese Academy of Sciences. The purpose of the experiment is to get the experience about the observing configuration of an FTS as well as its data reduction. The paper is arranged as follows. The principle of the FTS is described in Section 2, along with the brief introduction of our experimental system. The obtained interferograms and their inverted spectrum with our proposed method in the visible and near-IR wavelength are presented in Section 3, followed by the conclusion and future perspective part.

2 PRINCIPLE OF THE FOURIER TRANSFORM SPECTROMETER AND INTRODUCTION OF OUR EXPERIMENTAL SYSTEM

2.1 Principle of the Fourier Transform Spectrometer

Figure 1 shows the schematic diagram of a time-modulated FTS. The light beam from the solar telescope

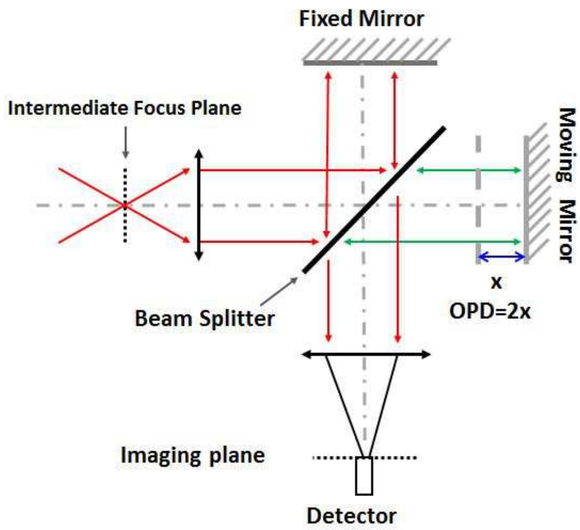

Fig. 1 Schematic diagram of a time-modulated FTS.

is firstly focused on the intermediate focal plane and then collimated by a collimating mirror. The collimated light beam further goes through the core part of an FTS, i.e., the Michelson interferometer compartment. The Michelson interferometer generally consists of a beam splitter, a fixed mirror and a moving mirror. The collimated light is divided by the beam splitter into the transmitting and reflecting beams. The transmitting light beam is reflected by the moving mirror and then reflected by the beam splitter (See the green arrows in Fig. 1), which has an optical path of L_1. The reflecting light beam is reflected by the fixed mirror and then goes through the beam splitter, having an optical path of L_2. Finally, two beams with different optical paths of L_1 and L_2, respectively, recombine into a single beam and interfere with each other. As the moving mirror moves along a precision-steel rod, the optical path L_1 varies with time. The optical path difference is different at different time, and a series of interference signals is recorded on the detector, forming the so-called interferogram.

For a polychromatic light, the relationship between the interferogram $I(L)$ and the target spectrum $B(\sigma)$ is (Bates 1978; Martin & Drissen 2017; Codding & Horlick 1973):

$$I(L) = \int_{-\infty}^{+\infty} B(\sigma)\cos(2\pi\sigma L)d\sigma, \tag{1}$$

where σ represents the wave number ($\sigma = 1/\lambda$, λ is the wavelength) and L is the optical path difference (OPD), i.e. $L_1 - L_2$. If we want to recover the target spectrum $B(\sigma)$ from Equation (1), the inverse Fourier cosine transform of the interferogram needs to be taken, as shown in Equation (2):

$$B(\sigma) = \int_{-\infty}^{+\infty} I(L)\cos(2\pi\sigma L)dL. \tag{2}$$

Table 1 Configurations of the Bruker IFS-125HR (New FTS Installed at HSOS)

wavelength range	beam splitter	Detector (material, size)
0.4–1.05 µm	Dielectric coating on Quartz	Silicon diode, 1 mm× 1 mm
0.91–5.4 µm	Si on CaF2	InSb detector (cooled with liguid N_2), 1 mm× 1 mm
1.6–16 µm	Ge on KBr	MCT detector (cooled with liguid N_2), 1 mm× 1 mm
2–25 µm	Ge on KBr	DLATGS detector, 1 mm×1 mm

From Equation (2) and the theory of Fourier transform, the highest spectral resolution of an FTS is determined by its maximum OPD, which depends on the maximum displacement x of the moving mirror (OPD=$2x$). In theory, the spectral resolution can be infinity. However, the longer displacement is, the more difficult to control the moving mirror. Moreover, the volume of an FTS is always finite in reality. So each FTS has a limited spectral resolution δB, which is proportional to $1/L$. In the case, Equation (2) becomes:

$$B(\sigma) = \int_{-L}^{+L} I(L)\cos(2\pi\sigma L)dL. \tag{3}$$

The relationship between the limited OPD and the full width at half maximum (FWHM) of the FTS instrument (or δB) is FWHM $= 0.6/L$ because the Fourier transform of a rectangular function (with a width of $2L$ from $-L$ to L) is a sinc function **(**$\sin L/L$**)**. The sampling resolution of an FTS is $\frac{1}{2L}$ from Equation (3). Due to the sidelobes or ringing effects of the sinc function, an apodization function is generally used to remove the effect with the sacrifice of reducing spectral resolution. The δB becomes $0.9/L$ for a triangular apodization function (Davis et al. 2001).

For AIMS, the required spectral resolution is 0.6 Å at 12.32 µm, corresponding to 0.004 cm^{-1}. If a triangular apodization function is used, the OPD is $0.9/0.004 = 225$ cm at least. The minimum displacement d of the moving mirror is 112.5 cm. So we selected an FTS from Bruker Corporation from Germany for our experimental system. Its production model is IFS-125HR, with a maximum OPD of 258 cm. The OPD can be configured from 0 to 258 cm, indicating that we can gather solar spectrum with different spectral resolution. It is worthy to mention that $I(L)$ is a continuous function in Equation (3). In reality, we has discrete sampling. Hence the equation can be rewritten below:

$$B(\sigma_j) = \sum_{j=-N}^{N} I(L_n)\cos(2\pi\sigma_j L_n), \tag{4}$$

where $I(L_n)$ is the interferogram obtained with the OPD of L_n and $B(\sigma_j)$ indicates the real spectrum at the wavenumber σ_j. The OPD between two adjacent sample interferogram, i.e., $L_{n+1} - L_n$, is the sampling interval $\delta_{\rm opd}$. N is the number of sampling points. The expression of the maximum OPD is : OPD $= \delta_{\rm opd} \times N$.

According to the Nyquist sampling theorem, the largest wavenumber σ_j is determined by the sampling interval $\delta_{\rm opd}$ with the relationship of $\sigma_j \leq \frac{1}{2\times\delta_{\rm opd}}$. That is to say, the obtained wavenumber range is from 0 to $\frac{1}{2\times\delta_{\rm opd}}$ in theory (or $2 \times \delta_{\rm opd} \leq \lambda \leq \infty$ with the wavelength unit). For a certain target wavelength, the best $\delta_{\rm opd}$ can be calculated with the above relationship. Generally, one can use a frequency stabilized laser worked in the visible wavelength to ensure equal interval sampling because the Fourier cosine transform of the laser is a cosine function. The laser wavelength $\lambda_{\rm laser}$ of Bruker IFS-125HR FTS is 632 nm and the useable $\delta_{\rm opd}$ is $N \times \frac{\lambda_{\rm laser}}{4}$. For example, the effective wavelength range is from 316 nm to ∞ in theory if the $\delta_{\rm opd}$ is set to $\frac{\lambda_{\rm laser}}{4}$. Larger $\delta_{\rm opd}$ is needed for longer wavelength.

From the above mentioned description, we summarized the advantage of an FTS. Firstly, one can observe solar spectrum with the required spectral resolution by setting appropriate OPD value. Secondly, it covers a broad wavelength range ($2 \times \delta_{\rm opd} \leq \lambda \leq \infty$) at a single measurement, which is limited by the $\delta_{\rm opd}$, the transmittance or reflectivity of the optical elements and the response range of the detector in reality. Thirdly, as theoretical longest wavelength of an FTS is infinity, it is more suitable for observing solar spectrum at longer wavelength with extremely high spectral resolution, e.g. the middle and far infrared wavelength. The moving mirror of an FTS generally moves along a precise guider rail and can easily move on the order of meters, resulting very large OPD and high resolution. Lastly, the rough wavelength calibration of an FTS is easy due to the equal interval sampling $\delta_{\rm opd}$ from the laser. Once the $\delta_{\rm opd}$ and the number of sampling points are determined, the OPD can be obtained. The wavenumber (wavelength) is also known after the Fourier cosine transform.

To better demonstrate the reason for the AIMS employing an FTS to observe solar spectrum, we compared an FTS with an Echelle grating spectrograph generally used for high spectral resolution observations in the visible and near-infrared wavelength. The longest wavelength of the Echelle grating spectrograph is determined by the grating constant *d* and the spectrum order *m* according to the grating equation,

$$2 \times d \times \sin\alpha = m\lambda, \tag{5}$$

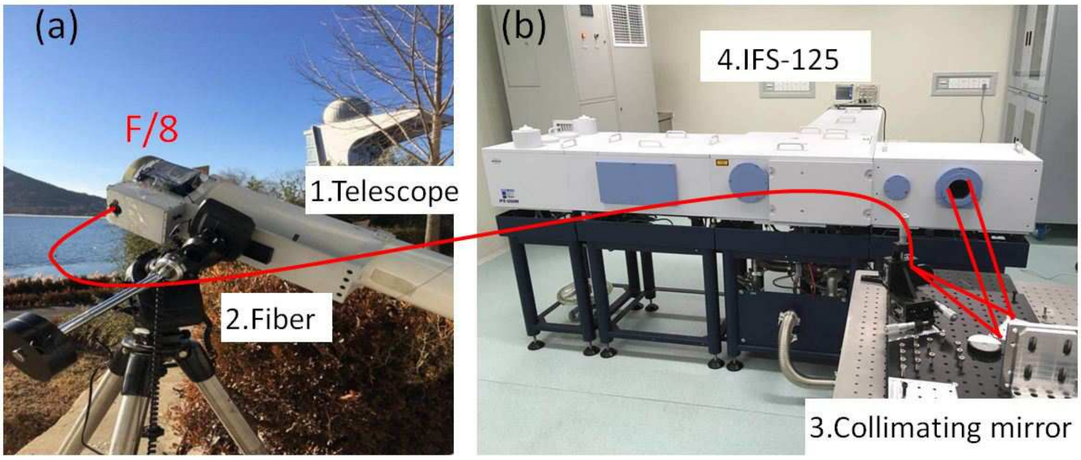

Fig. 2 The experimental system. (a): The equatorial and the Newtonian telescope. (b): The collimating mirror and the Bruker IFS-125HR FTS. The focuses of the telescope and the collimating mirror are flexibly linked by the fiber.

where α represents the blazing angle. For example, the largest wavelength occurs at the first spectrum order and equals to 31.645 µm for a grating with the d and α of 31.6 µm and 71 deg, respectively. To realize the needed resolution power of 205 333 for the AIMS at 12.32 µm, the required length of the grating is 133.9 cm if the theoretical power of $m \times N_{\rm grating}$ is used, where $N_{\rm grating}$ is the total number of the grating lines. Such a long grating is extremely difficult to manufacture.

2.2 Brief Introduction of Our Sun-light Feeding Experimental System and Newly Installed FTS

To get the experiences about the observing configuration of an FTS as well as its data reduction, we employed the Bruker IFS-125HR FTS with a point source detector. The FTS used for AIMS with a detector array of 64×2 is in development now. The equipped parameters of the Bruker IFS-125HR (see Fig. 2) are summarized in Table 1. Its maximal OPD is 258 cm and it has a broad spectral range of 0.4–25 µm by selecting different beam splitters and detectors. As a contrast, the maximal OPD of the FTS at McMath−Pierce Solar Facility is 100 cm, while its working spectral range is 0.2–20 µm (Brault 1972, 1978). So the Bruker IFS-125HR FTS has much longer OPD resulting in better spectral resolution in theory. As the spectral range of the fiber used in the current experimental system is 0.275 to 2.1 µm, only the visible and the near-IR solar spectrum can reach the FTS, which is presented in the following.

To feed the sunlight from visible to near-IR wavelength into our newly installed FTS at HSOS, we set up a temporary and simple experimental system. It contains a Newtonian reflector, a fiber, a collimating mirror and the FTS, as shown in Figure 2. The Newtonian reflector with an aperture of 10 cm and the focal ratio of 8, is installed on an equatorial platform to realize the pointing as well as the tracking to the Sun. A fiber with the core diameter of 320 µm and the numerical aperture of 0.22 is employed to flexibly connect the sunlight from the Newtonian reflector's focus to the focus of the collimating mirror. The sunlight is further collimated by the off-axis parabolic mirror and then enter the FTS. According to the focal ratio of the telescope and the core diameter of the fiber, the field of view of the gathered sunlight is about $82.5'' \times 82.5''$.

3 THE OBSERVED INTERFEROGRAM AND INVERTED SOLAR SPECTRUM IN THE VISIBLE AND NEAR-INFRARED WAVELENGTH

In the above section, we introduced the main principle of the FTS and our experimental system. The observed interferogram and its corresponding inverted solar spectrum are arranged in this section, following with a comparison with the solar spectrum atlas obtained by the FTS of National Solar Observatory (NSO), USA. During the observation, we do not use additional narrow band optical filters, so the broadband solar spectrum is obtained.

3.1 The Observed Solar Spectrum with the Bruker IFS-125HR FTS in the Visible Wavelength

We firstly try to take test observation in the visible wavelength. During the observation, the FTS is equipped with the Quartz beamsplitter and the silicon diolde detector listed in the first row of Table 1. The target wavelength range is 0.4–1.05 µm. The needed configurations of FTS

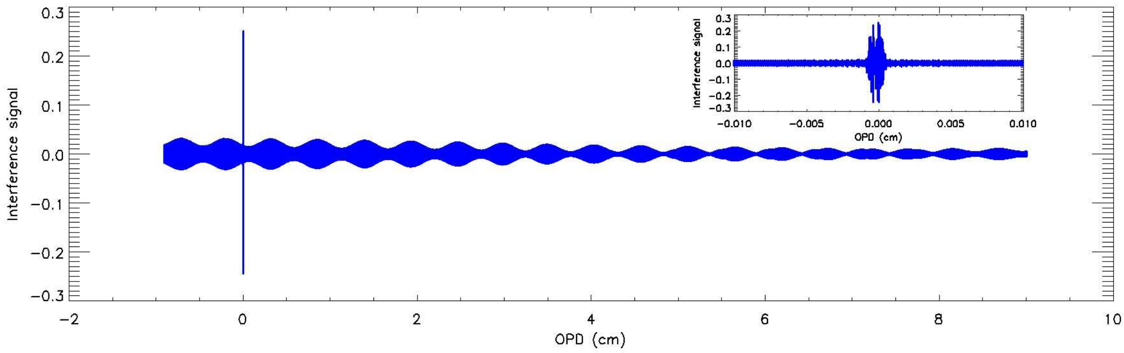

Fig. 3 Original interferogram taken from our experimental system for the visible wavelength. The subplot indicates the double side interferogram with the OPD from –0.01 to 0.01 cm.

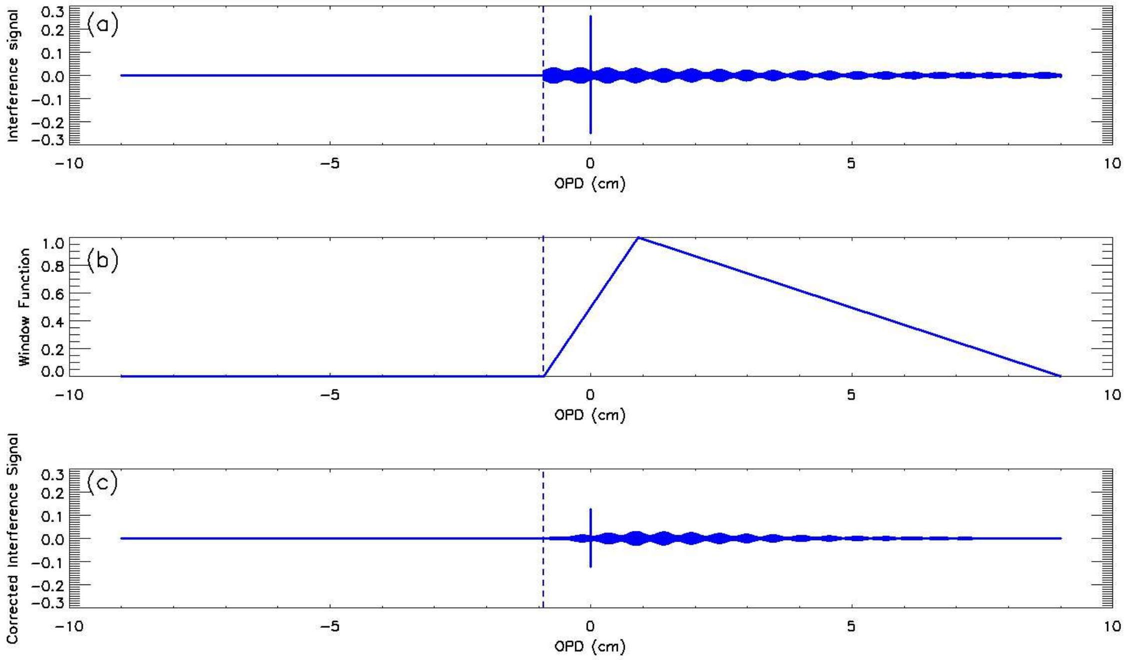

Fig. 4 Panel (a): Interferogram from Fig. 3 after zero filling. The regions on the left of the *dashed line* are filled with zero. Panel (b) is the triangular apodizing function. The interferogram after the process of apodization is shown in panel (c).

are the OPD, $\delta_{\rm opd}$, which is determined by the typical width of the visible solar spectrum and the principle of the FTS shown in Section 2. The $\delta_{\rm opd}$ is set to $\frac{\lambda_{\rm laser}}{4}$ because the selected shortest wavelength is 0.4 µm. The typical width of solar photospheric lines is about 0.1 Å, corresponding to $0.42\,{\rm cm}^{-1}$ at 0.48 µm. The one for the chromospheric lines is wider, which is about 0.3 Å (Moore et al. 1966). So the spectral resolution is set to be $0.1\,cm^{-1}$ here, with a maximal OPD of $0.9/0.1 = 9$ cm.

Generally the sampling OPD is from $-L$ to L according to Equations (3) and (4). Note that the Fourier cosine transform is an even function, indicating the interferogram between $-L$ to 0 equals to that from 0 to L. Hence the spectrum can be obtained even if we just gather half of the interferogram in theory. Half of the time can be saved in the case but with the same spectral resolution. However, an asymmetrical interferogram will result in phase shifts. A short interferogram from $-L_1$ ($L_1 \leq L$) to 0 can be taken then to correct the phase shift (Davis et al. 2001). The Bruker IFS-125HR employs such a configuration. So the interferogram with an OPD from –1 to 9 cm are taken here and the one from –1 to 1 cm is used for the phase shift correction. Considering the required $\delta_{\rm opd}$ is $\frac{\lambda_{\rm laser}}{4}$, the sampling numbers for one interferogram are OPD/$\delta_{\rm opd} = 6 \times 10^5$. The scanner velocity of the FTS is set to be $0.632992\,{\rm cm\ s}^{-1}$. The time taken for one scan is 15.7 s. As our FTS employs a photoconductive detector, the integral time cannot be manually configured.

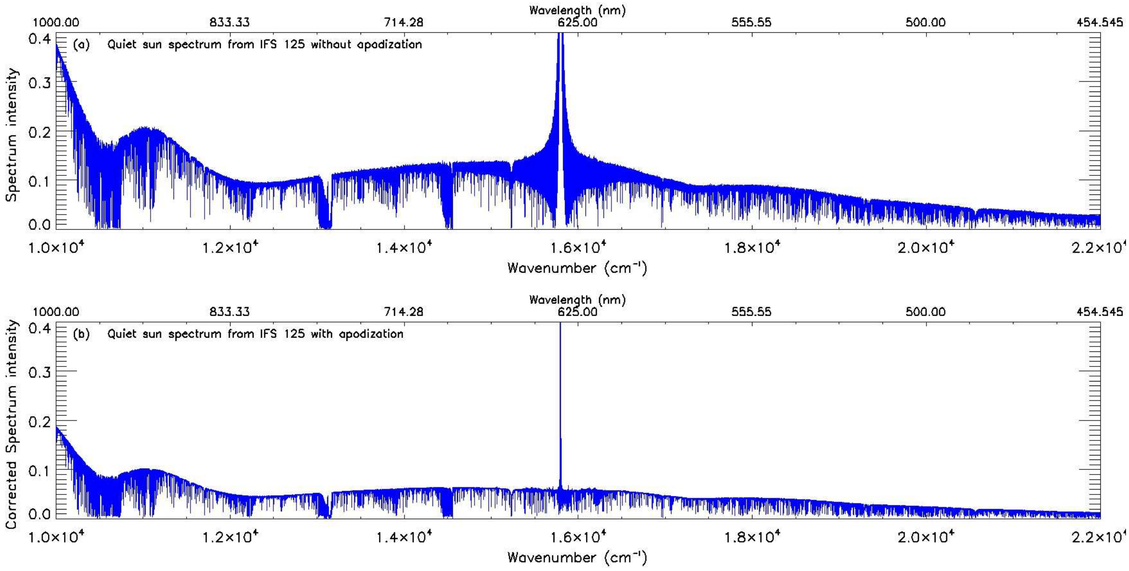

Fig. 5 The solar spectrum inverted from the interferogram in Fig. 4 in the range of 454.5 nm (22 000 cm^{-1}) to 1000 nm (10 000 cm^{-1}). The upper and lower panels are the one without and with the triangular apodizing functions.

With the above configurations of maximal OPD, $\delta_{\rm opd}$ and the short interferogram used for phase shift correction, we carried out test observation on 2018 Dec. 29, from 04:02 UT to 05:47 UT. Three hundred scans are added to improve the signal to noise ratio. The Bruker IFS-125HR can integrate interferogram for many scans. We take one hundred scans for one measurement and three measurements are used. The original unsymmetrical interferogram taken from all the three hundred scans can be found in Figure 3. The reduction from the interferogram to solar spectrum is listed step by step as follows.

– The OPD is extended to the range of –9 to 9 cm and the non-acquired interferogram between –9 and –1 cm is filled with zero. On one hand, we can use Equation (4) to invert the spectrum as well as its wavenumber value. On the other hand, the sampling resolution of the spectrum can be smaller since we elongated the length of the interferogram. The elongated interferogram after zero filling is arranged in Figure 4(a).
– Correction of the phase shift. We can rewrite the interferogram in Equation (6) considering the phase shifts.

$$I(L_n) = \sum_{j=-N}^{N} B(\sigma_j)\exp^{i(2\pi\sigma_j L_n+\phi_j)} = \sum_{j=-N}^{N} B(\sigma_j)\exp^{i\phi_j}\exp^{i2\pi\sigma_j L_n}\,. \tag{6}$$

Here ϕ_j presents the phase shift, which is nonzero if our sampling grid does not have the point that coincides with zero OPD. The unbalanced dispersion in either arm or the electronics system of the FTS can also introduce phase shifts.

The corresponding inverted spectrum $B(\sigma_j^1)$ is:

$$\begin{aligned} B(\sigma_j^1) &= B(\sigma_j)\exp^{i\phi_j} \\ &= \sum_{j=-N}^{N} I(L_n)\times\exp^{-i2\pi\sigma_j x_n} \\ &= B_{\rm re}(\sigma_j)+iB_{\rm im}(\sigma_j). \end{aligned} \tag{7}$$

Here $B(\sigma^1)$ is the inverse Fourier transformation of $I(L)$ other than the inverse Fourier cosine transform used in the ideal interferogram in Equation (2). $B_{\rm re}(\sigma_j)$ and $B_{\rm im}(\sigma_j)$ correspond to the real and image components of $B(\sigma^1)$, respectively. Regarding the phase shift ϕ_j, it can be determined from the double interferogram (Eq. (4)) with the limited OPD value from –l to 1 cm, according to the following equation:

$$\phi_j = \arctan(B_{\rm im}(\sigma_j), B_{\rm re}(\sigma_j)). \tag{8}$$

The solar spectrum $B(\sigma_j)$ has only real component. After eliminating the phase shift from the real interferogram, it can be obtained by combining Equations (7) and (8) (Davis et al. 2001):

$$B(\sigma_j) = Re\{B(\sigma_j^1)\exp^{-i\phi_j}\}. \tag{9}$$

Another way to correct the phase shift is employing the magnitude of the Fourier transformation. The inverted solar spectrum $B(\sigma_j)$ is :

$$B(\sigma_j) = \sqrt{B_{\rm re}^2(\sigma_j)+B_{\rm im}^2(\sigma_j)}. \tag{10}$$

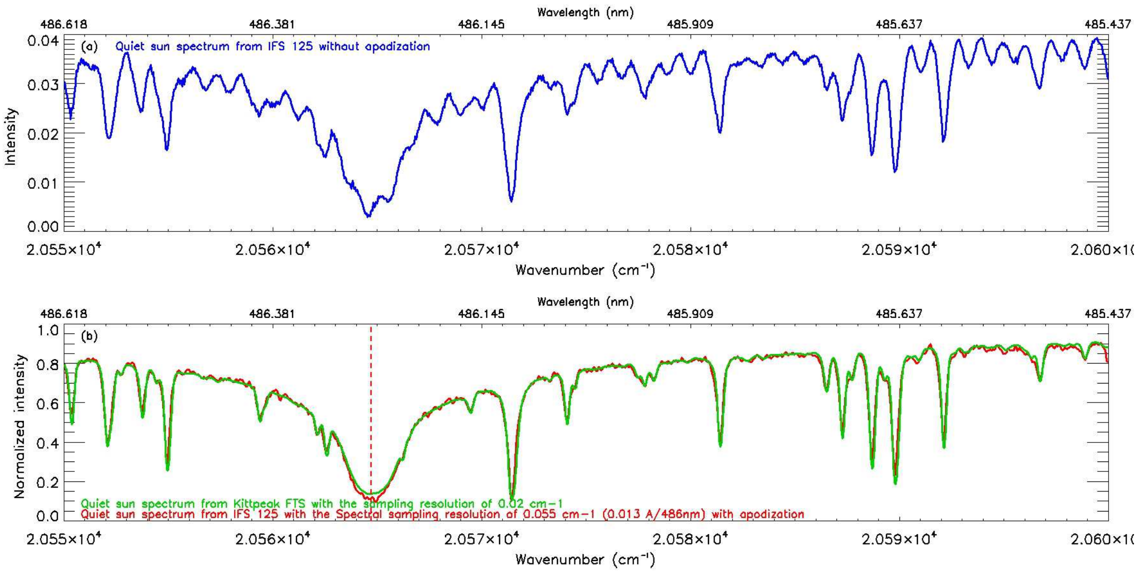

Fig. 6 The *blue line* in panel (a) and the *red one* in panel (b) are the quiet Sun spectrum near the Hβ line without and with the apodizing function extracted from Fig. 5(a) and (b), respectively. The continuum of the *red one* in panel (b) are normalized with the data taken by the FTS of NSO (*green line*) for comparison. The *dashed line* marks the linecenter of the Hβ line. The wavelength used here is vacuum wavelength. So the wavelength 486.1 nm in the air corresponds to 486.2 nm in the vacuum.

In the paper, we use the elongated interferogram in Figure 4(a) and Equation (10) to invert $B(\sigma_j)$. The inverted solar spectrum with the wavenumber selected from 10 000 cm^{-1} to 22 000 cm^{-1} is presented in Figure 5(a). With the known wavenumber from the Fourier transformation, we also obtained the corresponding spectral range, which is from 454.5 nm to 1000 nm. From Figure 5(a), we obtained the solar spectrum with a wide wavelength range just from a single interferogram. It is one of the advantage of the FTS. In contrast, tens of scans are needed to cover the same wavelength range for a grating spectrograph because only a narrow waveband is obtained for a single measurement. Moreover, many separate absorption lines exist in the inverted solar spectrum. Most of them are from the Sun while parts of the lines are from the absorption of the earth's atmosphere, which is not identified here. The wider lines in the spectrum correspond to the chromospheric spectral lines due to the higher temperature of the chromosphere, such as the famous Hα and Hβ lines with the central wavelength of 656.28 nm (15 237 cm^{-1}) and 486.1 nm (20 571 cm^{-1}), respectively. The bright line near 632.8 nm (15 802 cm^{-1}) is the reference laser used for realizing the same sampling interval $\delta_{\rm opd}$. We also chose a narrow wavelength range to check the profiles of a spectral line. The broad chromospheric Hβ line is selected and shown in Figure 6(a). The ringing effect due to the limited length of interferogram can be found.

– To remove the ring effect, a triangular apodizing function is employed. We multiplied the interferogram in Figure 4(a) by a triangular apodizing function seen in Figure 4(b). The resulting interferogram is presented in Figure 4(c). After the Fourier transformation, we obtained the corresponding solar spectrum with Equation (10). The one from 454.5 nm to 1000 nm can be found in Figure 5(b) and the selected one near the 486.1 nm is shown with the red line in Figure 6(b). Comparing the solar spectrum before and after employing the apodizing function, it clearly illustrates that most of the ring effect disappears.

In order to check the performance of the new installed FTS as well as the quality of our inverson algorithm, we selected parts of the inverted solar spectrum to compare with the solar atlas from the FTS obtained by NSO (Wallace et al. 1998). The broad chromospheric Hβ line is selected with a wavelength range of about 1.2 nm, from 485.4 nm (20 550 cm^{-1}) to 486.6 nm (20 550 cm^{-1}). Two steps are carried out before the spectrum are used for comparison. The nearby continuum from our inverted solar spectrum is firstly normalized to that from NSO with the green line in Figure 6(b). Then the two solar spectra are registered with each other. Because the wavenumber of the FTS is well determined by the OPD and the $\delta_{\rm opd}$, the shifted value for the registration is very small, which is 0.11 cm^{-1}. Comparing our observed solar spectrum near

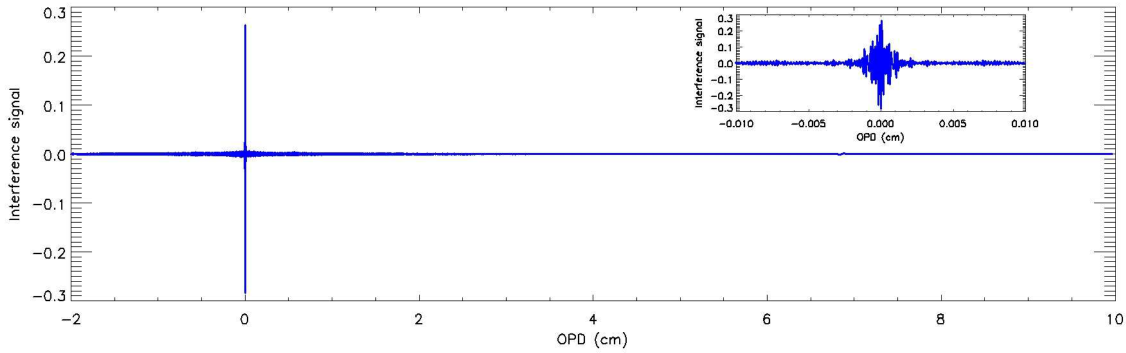

Fig. 7 Original interferogram taken from our experimental system for the near-infrared wavelength. The subplot indicates the double side interferogram with the OPD from –0.01 to 0.01 cm.

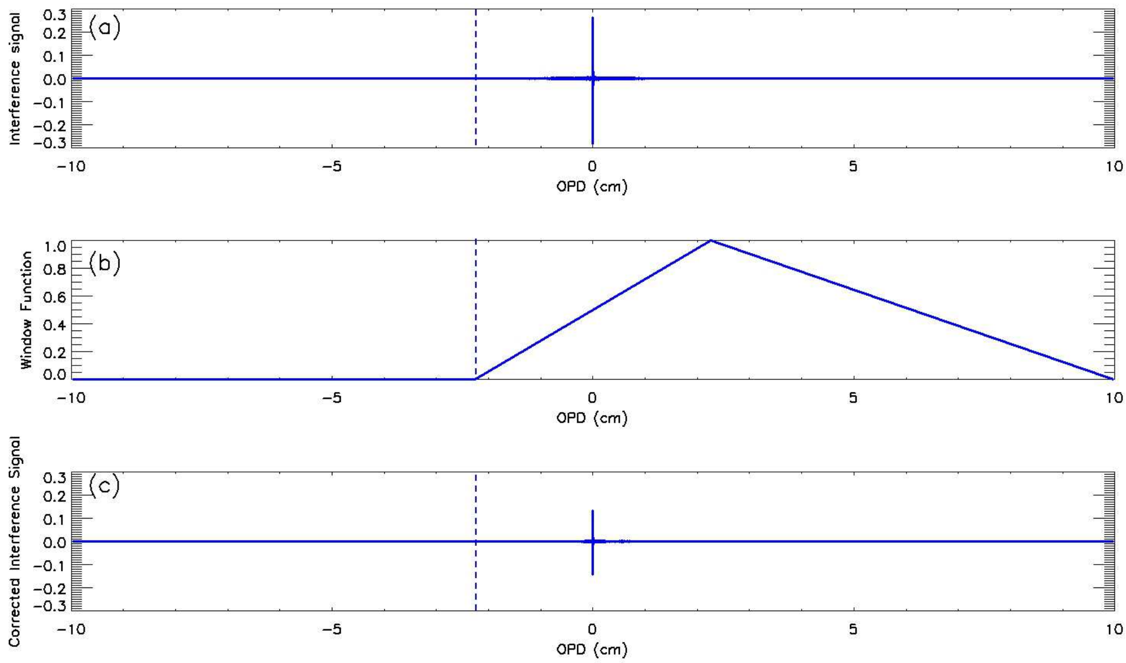

Fig. 8 From the upper to last rows, they are the interferogram from Fig. 7 with zero filling, the triangular apodizing function and the apodized interferogram, respectively.

Hβ line (red line) with that from NSO (green line), they agree very well with each other. Both the line depth and the line width of the broader Hβ line as well as the nearby narrow photospherical lines are almost the same. The difference is that our solar spectrum has much lower signal to noise ratio, which can be improved if we integrate a longer time.

3.2 The Observed Solar Spectrum with the Bruker IFS-125HR FTS in the Near-infrared Wavelength

We also carried out test observations for the wavelength from 1 μm (10 000 cm^{-1}) to 2.2 μm (4500 cm^{-1}). The longest wavelength 2.2 μm is limited by the transmittance of optical fibre. To cover the wavelength, the CaF_2 beam splitter and the InSb detector are employed, which are listed in the second row of Table 1. Again, we need to configure $\delta_{\rm opd}$, OPD and the short interferogram from $-L_1$ to 0 used for phase shift correction. As the shortest wavelength is 1 μm, the $\delta_{\rm opd}$ is set to be $\lambda_{\rm laser}/2$. One can also use $\lambda_{\rm laser}/4$ in principle at the expense of taking twice as much time as that with $\lambda_{\rm laser}/2$. The typical line width of the photoshperic lines near 1.5 μm is about 0.4 Å, corresponding to 0.18 cm^{-1}. The selected OPD is 10 cm here with a spectral resolution of $0.9/10 = 0.09$ cm^{-1} if a triangular apodizing function is employed according to the principle describe in Section 2. L_1 is set to be –2 cm here. So the interferogram is taken form –2 cm to 10 cm.

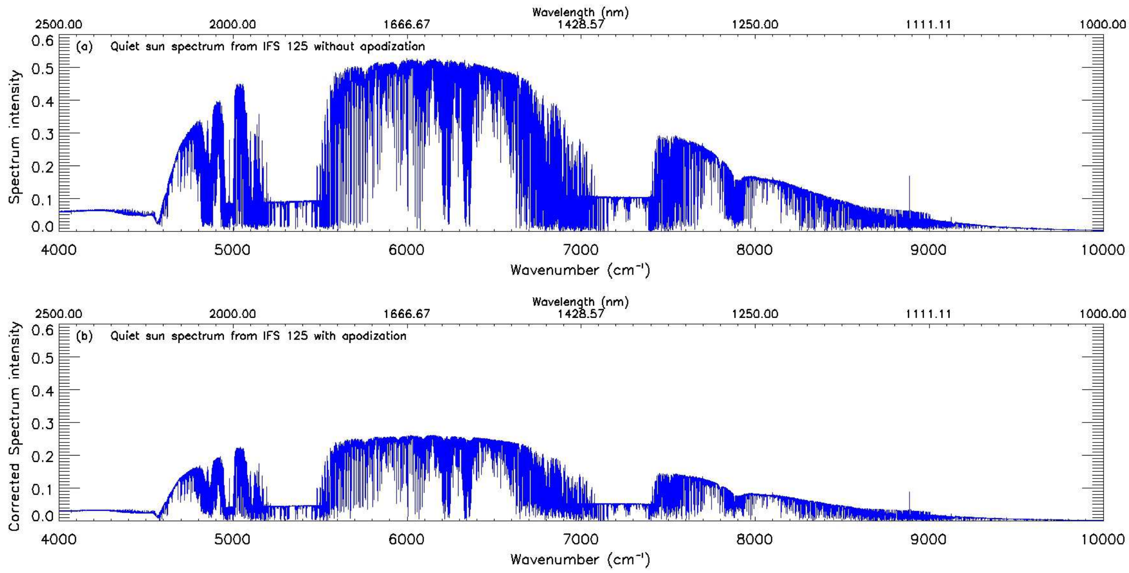

Fig. 9 The solar spectrum inverted from the interferogram in Fig. 8 in the range of 1000 nm (10 000 cm^{-1}) to 2222 nm (4500 cm^{-1}). The upper and lower rows are those without and with apodizing function.

The observation was taken on 2019 Jan. 01, from 04:50 UT to 05:56 UT. One hundred scans are added to improve the signal to noise ratio. The original interferogram is arranged in Figure 7. The data reduction of the interferogram is the same as that in the visible wavelength. First, the values of the interferogram with the OPD from –10 cm to –2 cm are filled with zero, as seen from Figure 8(a). Then it is multiplied by a triangular apodizing function in Figure 8(b). The interferogram after apodization is presented in Figure 8(c). We take the Fourier transform of the interferogram with and without apodizing function and the corresponding solar spectrum from 1 μm to 2.2 μm calculated with Equation (10) is shown in Figure 9(a) and 9(b), respectively. We can find that the solar spectrum with apodization has lower intensity. Similar with the spectrum in Figure 5, there are many narrow isolated spectral lines from solar photosphere and some broad spectral lines mainly from the molecular absorption band of the earth atmosphere. For example, the absorption near the wavenumber of 7150 cm^{-1} (1.4 μm) and 5250 cm^{-1}(1.9 μm) are mainly from the absorption of the water vapour (Hinkle et al. 2003).

Finally, we compared our observed solar spectrum with that from the FTS belonging to NSO and the result was shown in Figure 10 (Livingston & Wallace 1991). The selected spectral line is Fe I 1.56 μm, which is used by many solar telescopes for the accurate measurement of photospherical magnetic field (Collados et al. 2012; Cao et al. 2010; Liu et al. 2014). The wavelength range is about 4.8 nm. The continuum is also normalized to that from NSO. The shifted value of the wavenumber is 0.045 cm^{-1} during the registration of the two spectrum. Comparing our inverted solar spectrum before (Fig. 10(a))and after employing apodizing function (red line in Fig. 10(b)), the ring effect is removed. From the comparison between the red (our inverted solar spectrum) and the green line that from NSO in Figure 10(b), both the line depth and the line width are nearly the same. The signal to noise ratio observed by us is also lower due to the smaller aperture of the light-feeding telescope.

4 CONCLUSION AND FUTURE PERSPECTIVE

We installed a Bruker IFS-125HR FTS at HSOS with a maximum OPD of 258 cm. The wavelength range is from 0.4 μm to 25 μm, covering the visible, near and mid-infrared wavelength. As an FTS has never used by any solar telescopes in China, we established a temporary sunlight feeding system and tried to gather experience both for the observing configuration and the data inversion from interferogram to solar spectrum. The work shown here is useful for the data reduction of the AIMS telescope, which also uses an FTS and will obtain its first light near 2022.

We firstly introduced the principle of a time-modulated FTS and showed that it is more suitable for realizing the spectral resolution of the AIMS. We summarized the main advantages of an FTS. Firstly, it is more suitable for the longer wavelength, e.g., the middle and far infrared waveband. Secondly, it is easy to reach very high spectral-resolution and the resolution can be set optionally by the user. Thirdly, it has broad wavelength range. Lastly, an FTS can give the wavelength value because it has a frequency stabilized laser resulting the well known OPD. The necessary observing configurations

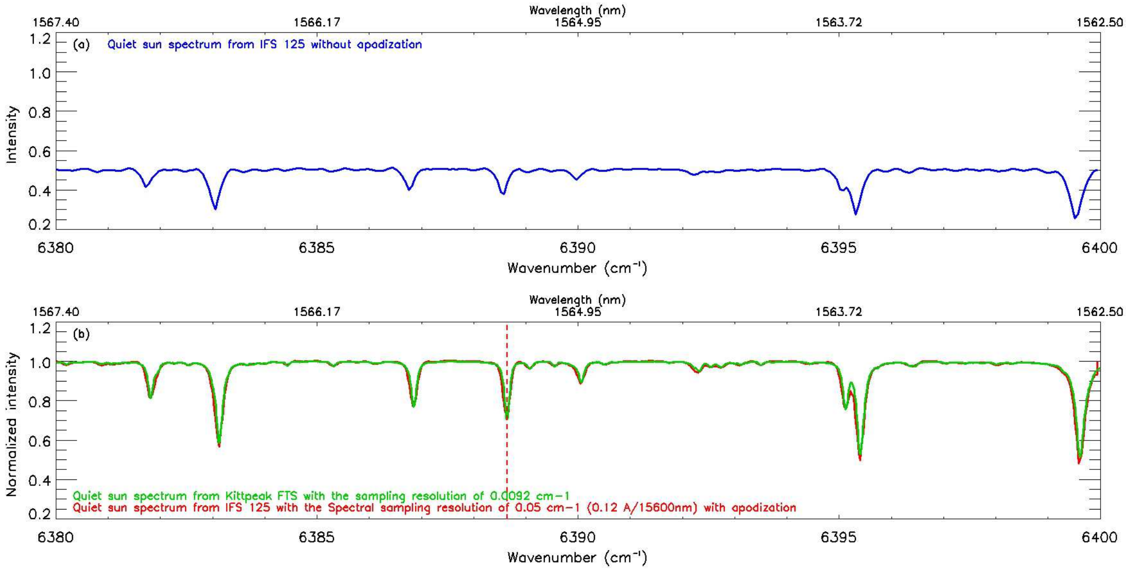

Fig. 10 Similar with Fig. 6 but for the region near the Fe I 1.56 μm line. Panel (a) and the *red line* in panel (b) are the spectrum extracted from Fig. 9(a) and 9(b), respectively. The *green line* are the data taken by the FTS of NSO. The *dashed line* marks the linecenter of the Fe I 1.5648 μm line. The wavelength is also vacuum wavelength.

needed for an FTS when taking solar spectrum are the appropriate $\delta_{\rm opd}$, maximal OPD as well as the OPD value used for phase shift correction. Also, the directly observed quantity of an FTS is the interferogram. So the Fourier transformation must be employed to recover the solar spectrum.

We carried out test observations with our experimental system in the visible and near-infrared wavelength. According to the target wavelength range and the typical width of the solar spectral lines, we determined the suitable $\delta_{\rm opd}$, maximal OPD as well as the OPD value used for phase shift correction. The interferogram is obtained then. Considering the asymmetric interferogram, infinite OPD and the phase shift in our interferogram, we firstly filled the zero value to make a symmetric interferogram with the OPD from $-L$ to L. Then a triangular apodizing function is multiplied by the interferogram to reduce the ring effect. The final spectrum is the magnitude from the Fourier transformation of the interferogram to correct the phase shift.

With the Bruker IFS-125HR FTS, we successfully obtained the broadband solar spectrum from 0.45 μm to 2.2 μm. Two common used spectral lines, i.e., chromospherical Hβ 486.1 nm in the visible and photospherical Fe I 1.56 μm lines in the near infrared, are compared with those taken from the FTS by NSO. Both the line depth and width are almost the same except a relatively lower signal to noise ratio in the solar spectrum taken by our FTS. The comparison results confirm the effectiveness of our observing configuration and data reduction method.

We would like to emphasize that the results shown here just focus on the visible and near-infrared wavelength range mainly due to the limited transmittance profile of the optical fiber. The line width of the solar spectrum is not narrow enough to calibrate the practical spectral resolution of the FTS, indicating we need to find other calibration methods. The data reduction from interferogram to solar spectrum is a preliminary result as well. What is the best apodizing function for the inversion of a solar spectrum? What decides the OPD to derive the phase shift? Is it possible to use Equation (9) to correct the phase shift? What is the relationship between the scan time and the signal to noise ratio? These questions need to be further investigated. Moreover, the maximal OPD used in the paper is only 10 cm, much less than the maximal OPD of 258 cm. If the solar spectrum is observed in the mid-infrared, e.g., the wavelength range of 10–13 μm selected by the AIMS, we need longer OPD. It is also well known that many spectral lines from earth atmosphere exist in the mid-infrared (Hinkle et al. 2003). The radiation from the instrument, the nearby background and the earth atmosphere contribute a lot in the mid-infrared wavelength. So we need to identify and find a method to correct them. Based on the above considerations, an upgraded experimental system with all reflected mirrors is under construction at HSOS by now. The diameter of its primary mirror is 60 cm. The solar spectrum from 2.2 to 25 μm with more photons can be taken then, which is helpful for addressing the above remaining problems.

Acknowledgements We sincerely thank the referee for helpful suggestions that greatly improved the manuscript.

We are also grateful for Prof. Kaifan Ji and Song Feng for the discussions on the theory of Fourier transform. This research work is supported by the National Natural Science Foundation of China (Grant Nos. 11873062, 11427901, 11673038, 11803002, 11973056, 11973061, 12003051 and 12073040). We are also supported by the Strategic Priority Research Program of the Chinese Academy of Sciences (Grant Nos. XDA15320102 and XDA15052200).

References

Ai, G. 1993, in Astronomical Society of the Pacific Conference Series, 46, IAU Colloq. 141: The Magnetic and Velocity Fields of Solar Active Regions, eds. H. Zirin, G. Ai, & H. Wang, 149
Ayres, T. R. 2002, ApJ, 575, 1104
Bates, J. B. 1978, Computers Mathematics with Applications, 4, 73
Brault, J. 1972, in Auxiliary Instrumentation for Large Telescopes, 367
Brault, J. W. 1978, in Future Solar Optical Observations Needs and Constraints, ed. G. Godoli, 106, 33
Bruls, J. H. M. J., Solanki, S. K., Rutten, R. J., & Carlsson, M. 1995, A&A, 293, 225
Cao, W., Gorceix, N., Coulter, R., et al. 2010, Astronomische Nachrichten, 331, 636
Chang, E. S., & Noyes, R. W. 1983, ApJL, 275, L11
Codding, E. G., & Horlick, G. 1973, Applied Spectroscopy, 27, 85
Collados, M., López, R., Páez, E., et al. 2012, Astronomische Nachrichten, 333, 872
Davis, S. P., Abrams, M. C., & Brault, J. W. 2001, Fourier Transform Spectrometry (Academic Press)
del Toro Iniesta, J. C., & Ruiz Cobo, B. 2016, Living Reviews in Solar Physics, 13, 4
Deng, Y., Liu, Z., Qu, Z., Liu, Y., & Ji, H. 2016, in Astronomical Society of the Pacific Conference Series, 504, Coimbra Solar Physics Meeting: Ground-based Solar Observations in the Space Instrumentation Era, eds. I. Dorotovic, C. E. Fischer, & M. Temmer, 293
Fang, C., Chen, P.-F., Jiang, R.-L., & Tang, Y.-H. 2010, RAA (Research in Astronomy and Astrophysics), 10, 83
Farmer, C. B. 1994, in Infrared Solar Physics, ed. D. M. Rabin, J. T. Jefferies, & C. Lindsey, 154, 511
Farmer, C. B., & Norton, R. H. 1989, A High-resolution Atlas of the Infrared Spectrum of the Sun and the Earth Atmosphere from Space(National Aeronautics and Space Administration, Hampton, VA (USA), Langley Research Center)
Feng, S., Deng, Z., Yuan, D., Xu, Z., & Yang, X. 2020, RAA (Research in Astronomy and Astrophysics), 20, 117
Hase, F., Wallace, L., McLeod, S. D., et al. 2010, J. Quant. Spec. Radiat. Transf., 111, 521
Hinkle, K. H., Wallace, L., & Livingston, W. 2003, in Bulletin of the American Astronomical Society, 35, 1260
Li, Y., Kelly, M., Ding, M. D., et al. 2017, ApJ, 848, 118
Li, D., Yang, X., Bai, X. Y., et al. 2020, A&A, 642, A231
Liu, Z., Xu, J., Gu, B.-Z., et al. 2014, RAA (Research in Astronomy and Astrophysics), 14, 705
Livingston, W., & Wallace, L. 1991, An Atlas of the Solar Spectrum in the Infrared from 1850 to 9000 cm^{-1} (1.1 to 5.4 micrometer) (NSO Technical Report, Tucson: National Solar Observatory, National Optical Astronomy Observatory)
Martin, T., & Drissen, L. 2017, arXiv e-prints, arXiv:1706.03230
Moore, C. E., Minnaert, M. G. J., & Houtgast, J. 1966, The Solar Spectrum 2935 A to 8770 A (ational Bureau of Standards Monograph, Washington: US Government Printing Office (USGPO))
Penn, M. J. 2014, Living Reviews in Solar Physics, 11, 2
Rimmele, T. R., Warner, M., Keil, S. L., et al. 2020, Sol. Phys., 295, 172
Socas-Navarro, H., de la Cruz Rodríguez, J., Asensio Ramos, A., Trujillo Bueno, J., & Ruiz Cobo, B. 2015, A&A, 577, A7
Solanki, S. K., Livingston, W., & Ayres, T. 1994, Science, 263, 64
Solanki, S. K., Inhester, B., & Schüssler, M. 2006, Reports on Progress in Physics, 69, 563
Tennyson, J. 2011, Astronomical Spectroscopy: AN Introduction to the Atomic and Molecular Physics of Astronomical Spectra (2ND Edition) (World Scientific)
Uitenbroek, H., Noyes, R. W., & Rabin, D. 1994, ApJL, 432, L67
Wallace, L., Hinkle, K., & Livingston, W. 1998, An Atlas of the Spectrum of the Solar Photosphere from 13,500 to 28,000 cm^{-1} (3570 to 7405 A) (Tucson, AZ: National Optical Astronomy Observatories)
Xu, Z., Hénoux, J. C., Chambe, G., et al. 2005, ApJ, 631, 618